Influence of the Turbulence Closure Scheme on the Finite-Element Simulation of the Upwelling in the Wake of a Shallow-Water Island

Sébastien Blaise [a,*], Eric Deleersnijder [b,c], Laurent White [c,b] and Jean-François Remacle [a,c]

[a] *Université catholique de Louvain, Unité de Génie Civil et Environnemental, B-1348 Louvain-la-Neuve, Belgium*

[b] *Université catholique de Louvain, Institut d'Astronomie et de Géophysique G. Lemaître, B-1348 Louvain-la-Neuve, Belgium*

[c] *Université catholique de Louvain, Centre for Systems Engineering and Applied Mechanics (CESAME), B-1348 Louvain-la-Neuve, Belgium*

Continental Shelf Research 27 (2007), 2329-2345

doi:10.1016/j.csr.2007.06.003

Abstract

A three-dimensional finite-element model is used to investigate the tidal flow around Rattray Island, Great Barrier Reef, Australia. Field measurements and visual observations show both stable eddies developing at rising and falling tide in the wake of the island. The water turbidity suggests intense upwelling able to carry bed sediments upwards. Based on previous numerical studies, it remains unclear at this point whether the most intense upwelling occurs near the centre of the eddies or off the island's tips, closer to the island. All these studies resorted to a very simple turbulence closure, with a zero-equation model whereby the coefficient of vertical viscosity is computed via an algebraic expression. In this work, we aim at studying the influence of the turbulence closure on model results, with emphasis on the prediction of vertical motions. The Mellor and Yamada level 2.5 closure scheme is used and an increase in the intensity of vertical transport is observed. This increase is partly explained by the fact that the Mellor and Yamada model takes into account the hysteresis effect in the time variation of turbulence variables. The influence of the advection of turbulence variables is estimated to be negligible. By a better representation of transient coastal phenomena, the Mellor and Yamada level 2.5 turbulence closure improves the model to a significant degree.

Key words: Finite Element Method, Turbulence closure scheme, Upwelling, Lee eddies, Shelf dynamics, Tidal currents, Unstructured mesh, Australia, Great Barrier Reef, Rattray Island

1 Introduction

Over the last decade, increasing effort has been directed toward the development of marine models using unstructured meshes. A thorough review of these studies is presented by Pain et al. (2005). Admittedly, unstructured meshes have much to offer for marine modelling. They allow for an accurate representation of the topography (e.g., islands, narrow straits) and the bathymetry (Legrand et al., 2007, 2006). The mesh can easily be refined in regions of interest or coarsened in those regions where the dynamics is less demanding. Finally, unstructured meshes set up in spherical geometry should be able to circumvent the singularity at the poles, rendering those techniques potentially very useful for global scale ocean modelling (Legrand et al., 2000; Gorman et al., 2006). These assets are quite compelling for marine modelling and should prompt further developments and research for improving current models. Several numerical methods can handle unstructured meshes; among them the finite volume method, the spectral element method and the finite element method. In this paper, we focus on the finite element (FE) method.

The first developments of FE marine models were based on the wave continuity equation (Lynch and Gray, 1979), whereby the primitive shallow-water equations are manipulated to form a wave equation to predict the free-surface elevation. This method does not suffer from spurious oscillations occurring when using equal-order interpolations with the primitive equations. The generalisation of this method led to the generalised wave continuity equation (GWCE), documented by Kinnmark (1986). The GWCE has been extensively used over the past 20 years with successful applications in coastal regions for tidal predictions (Walters and Werner, 1989; Lynch and Naimie, 1993; Lynch et al., 1996; Fortunato et al., 1997; Cushman-Roisin and Naimie, 2002). This method, however, is subject to advective instabilities (Kolar et al., 1994) and suffers from the breaking down of mass conservation (Massey and Blain, 2006), making it less suitable for coupling with transport equations and long-term integrations.

These limitations urged the development of marine models based on the primitive equations. To that end, research toward finding a stable mixed FE formulation for the shallow-water equations has been thriving since the end of the nineties (Le Roux et al., 1998; Le Roux, 2001; Hanert et al., 2003; Le Roux, 2005). Early issues of the FE method, often cited as pretexts not to use it, are starting to lose resilience. Nowadays, developments and applications of FE marine models based on the primitive equations are becoming less of an exception (Nechaev et al., 2003; Danilov et al., 2004; Ford et al., 2004a,b;

* Corresponding author.
Email address: sebastien.blaise@uclouvain.be (Sébastien Blaise).

Danilov et al., 2005; Hanert et al., 2005; Labeur and Pietrzak, 2005; Pain et al., 2005; Pietrzak et al., 2005, 2006; Walters, 2006; White and Deleersnijder, 2006; White et al., 2007). This revolution in model design calls for validation test cases. Idealised test cases are generally too simple and are usually set up to validate the numerical component of a model without too much regard onto the ability of the model to represent the physics. There is a great need of realistic test cases against which models can assess their ability at representing processes encountered in the field. With this objective in mind, a self-forming group is putting together a set of realistic benchmarks that ought to remain relevant for the next decade (Aikman et al., 2006). Following these guidelines, Blaise and White (2006) recently set up a benchmark focusing on the three-dimensional flow around Rattray Island, Great Barrier Reef, Northeast Australia (Figure 1).

In 1982, the Australian Institute of Marine Science carried out an extensive field survey at Rattray Island (Wolanski et al., 1984). Twenty-six current-meters were deployed at various sites in the southeast of the island and the water elevation was recorded. Landsat imagery and aerial photographs allow for direct visualisation of the secondary circulation in the wake of the island. The recirculating water is turbid, facilitating the interpretation of the circulation from the air. Since then, Rattray Island has been the focus of several studies (Falconer et al., 1986; Black and Gray, 1987; Wolanski and Hamner, 1988; Deleersnijder et al., 1992; Wolanski et al., 1996; White and Deleersnijder, 2006; White et al., 2007), all of them but the last using the finite difference method. By using a finite element model, White and Deleersnijder (2006) aimed at investigating the effect of an increase in mesh resolution, keeping all other parameterisations identical to that used in previous studies using the finite difference method (Deleersnijder et al., 1992; Wolanski et al., 1996). In this paper, the same FE model is utilised but it is improved with a more sophisticated turbulence closure.

Vertical mixing by turbulence is a key player in the dynamics of processes encountered in shallow coastal areas (Burchard, 2002). Simple turbulence closures, such as that used by Deleersnijder et al. (1992) and White and Deleersnijder (2006), neglect parts of the complex evolution of turbulent flows. In this paper, the Mellor and Yamada level 2.5 turbulence closure (MY25) (Mellor and Yamada, 1974, 1982) is considered mainly because it was designed and tuned for geophysical fluid flow problems. Moreover, this turbulence closure has been widely used in marine models (e.g. Blumberg and Galperin, 2006; Ruddick et al., 1995; Ezer, 2005; Timmermann and Losch, 2005) and was recently implemented in a FE water column model (Hanert et al., 2006). With a better parameterisation of turbulence, we seek to improve the prediction of the flow around Rattray Island and, in particular, the representation of the upwelling mechanisms. By carrying the sediments from the sea bed to the sea surface, an intense upwelling could be a dominant factor explaining the water

turbidity in the wake of the island. Previous numerical models gave an insufficient upwelling velocity in the wake of the island. It was initially thought that the resolution of the models was insufficient (Deleersnijder et al., 1992); but recent finite-element simulations with variable horizontal resolutions (White and Deleersnijder, 2006) showed that the resolution was not in question. In that study, the authors used a diagnosis of vertical transport based on the age of the bottom water, that can be considered to be the time elapsed since a constituent left the sea bottom (Delhez et al., 1999; Deleersnijder et al., 2001). Their results allow for concluding that upwelling also occurs off the island's tips (very close to the island) and not only near the centre of the eddies. Moreover, they found that upwelling off the island's tips was the most intense. However, the upwelling predicted by the model was not always sufficient to explain the presence of sediments at the sea surface. The turbulence closure used in their study was admittedly too simple. Therefore, it remains unclear whether the most significant upwelling mechanisms occur off the island's tips or near the centre of the eddies.

In this paper, after introducing the upwelling velocity we will describe the model and the parameters used to perform the simulations. Sections 4 to 7 will be devoted to the results of simulations and comparisons using different parameterisations of turbulence. The last section before the conclusion will estimate the importance of the advection of turbulence variables in the model applied to Rattray Island.

2 Upwelling velocity within eddies

The quantitative assessment of vertical motions calls for a representative estimator. In this work, the intensity of vertical transport will be estimated by using the so-called upwelling velocity (Deleersnijder, 1989, 1994). The upwelling velocity is not directly influenced by the bathymetry but is entirely due to upwelling mechanisms. Let us consider the following transformation to σ-coordinates:

$$\sigma = \frac{z - \eta}{h + \eta}, \tag{1}$$

where h and η are respectively the unperturbed sea depth and the sea surface elevation, positive upwards. The vertical coordinate z is pointing upward with its origin at the mean sea level. The upwelling velocity is the component of the vertical velocity that modifies the relative position of a particle within the water column, i.e. the vertical velocity component that allows a particle to cross iso-sigma surfaces. In this study, we will focus on the upwelling velocity, and the transport by turbulent mixing will not be included in the diagnoses. White and Deleersnijder (2006) showed that the upwelling velocity is presumably a dominant process in the rise of sediments.

Upwelling mechanisms in an eddy configuration are represented in Figure 2. The velocity of the fluid on the perimeter of the eddy is smaller near the sea bed (u_{bottom}) than near the sea surface (u_{top}) because of bottom friction. The rotating fluid is sustained by a centrifugal acceleration in equilibrium with the pressure gradient induced by the slope of the sea surface. Close to the sea bed and because of bottom friction, the centrifugal acceleration magnitude decreases while the pressure gradient remains constant and this balance breaks down. This leads to flow convergence near the seabed and upwelling within the centre of the eddy. On the outer edge of the eddy, the centrifugal acceleration leads to a convergence of the flow at the sea surface, inducing downwelling. Thus, shallow-water eddies tend to induce upwelling at the centre and downwelling along the outer edge. The upwelling mechanism in eddies is similar to that occuring in a stirred tea cup, with a convergent flow near the bottom and upwelling in the centre (Bowker, 1988; Wolanski et al., 1996). In this work, we will focus on upwelling zones. According to the foregoing explanations, the larger the difference between the bottom velocity and the surface velocity, the larger the upwelling in the centre of the eddy.

3 Model description

We use the three-dimensional finite-element marine model developed within the scope of the SLIM project (Second-generation Louvain-la-Neuve Ice-ocean Model, http://www.climate.be/SLIM). A version of the model SLIM, using sigma coordinates and considering a constant density, is described in detail by White et al. (2007) and the configuration used for studying the flow around Rattray Island is presented by White and Deleersnijder (2006). It is very briefly recalled here. According to Wolanski et al. (1984), temperature and salinity contrasts are negligible near Rattray Island. Therefore, we consider the water to have a constant density. We work on an f-plane and under the hydrostatic approximation. Wind stress is not considered. The same assumptions as those of White and Deleersnijder (2006) are made here so that the only difference between both models is the turbulence closure.

The horizontal momentum equation is then

$$\frac{\partial \mathbf{u}}{\partial t} + (\mathbf{v} \cdot \nabla)\,\mathbf{u} + f\widehat{\mathbf{e}}_{\mathbf{z}} \wedge \mathbf{u} = -g\nabla_h \eta + \frac{\partial}{\partial z}\left(\nu_v \frac{\partial \mathbf{u}}{\partial z}\right) + \mathbf{D}, \tag{2}$$

where $\mathbf{v} = (u, v, w)$ is the velocity and $\mathbf{u} = (u, v)$ contains the horizontal components of $\mathbf{v}$. The three-dimensional gradient operator is designated by ∇; ∇_h is used to designate the horizontal gradient operator, which applies on the horizontal components of a vector. The constant Coriolis parameter and the gravitational acceleration are respectively represented by f and g; ν_v

and $\widehat{\mathbf{e}}_\mathbf{z}$ are respectively the vertical eddy viscosity coefficient and the upward-pointing unit vector. In the scope of this work, the vertical eddy viscosity will be calculated by means of different turbulence closure schemes in order to investigate their effect on the results. $\mathbf{D}$ is the parameterisation of horizontal momentum diffusion. In addition to equation (2), the continuity equation is used to diagnostically compute the vertical velocity:

$$\frac{\partial u}{\partial x} + \frac{\partial v}{\partial y} + \frac{\partial w}{\partial z} = 0. \tag{3}$$

The free-surface elevation equation is derived from

$$\frac{\partial \eta}{\partial t} + \nabla_h \cdot \left(\int_{-h}^{\eta} \mathbf{u} \mathrm{d}z \right) = 0. \tag{4}$$

The total height of the water column is defined as $H(x, y, t) = h(x, y) + \eta(x, y, t)$. The horizontal momentum diffusion term $\mathbf{D}$ is

$$\mathbf{D} = \frac{\partial}{\partial x}\left(\nu_h \frac{\partial \mathbf{u}}{\partial x} \right) + \frac{\partial}{\partial y}\left(\nu_h \frac{\partial \mathbf{u}}{\partial y} \right), \tag{5}$$

in which ν_h is computed using a Smagorinsky scheme (Smagorinsky, 1963)

$$\nu_h = c_s \triangle^2 \left[\frac{\partial \overline{u}}{\partial x}\frac{\partial \overline{u}}{\partial x} + 0.5\left(\frac{\partial \overline{u}}{\partial y} + \frac{\partial \overline{v}}{\partial x} \right)^2 + \frac{\partial \overline{v}}{\partial y}\frac{\partial \overline{v}}{\partial y} \right]^{\frac{1}{2}}, \tag{6}$$

where c_s is a constant and Δ^2 is a the surface area of the local triangle (Akin et al., 2003). The overbar stands for depth-averaged quantities.

In this paper, the domain geometry, boundary conditions and forcings are identical for all simulations.. The tidal ellipses are strongly polarised (Wolanski et al., 1984) and a good approximation consists in assuming the mean flow to be unidirectional. The domain is rotated so that its y-axis is parallel to the direction of the tidal flow. Lateral boundaries are then assumed to be impermeable, without lateral friction. The southeast and northwest boundaries remain open. On the open boundaries, the depth-averaged velocity and the elevation obtained from field measurements are imposed under the form of the incoming characteristic variable $\overline{u}_n - \eta\sqrt{g/h}$ where $\overline{u}_n$ is the depth-averaged normal velocity (Flather, 1976; Ruddick et al., 1994). The phase lag between incoming and outgoing boundaries is neglected. The size of the domain is $8,2km$ in the x-direction and $12,1km$ in the y-direction.

Two different unstructured meshes, refined in the vicinity of the island, are employed. The coarse mesh is made of 3024 triangles and 10 layers on the vertical (Figure 3). Its horizontal resolution varies from $140m$ in the vicinity of the island to $700m$ near the domain boundaries. The fine mesh comprises

6096 triangles and 16 layers on the vertical. Its horizontal resolution in the vicinity of the island is $85m$ whereas the resolution near the domain boundaries is unchanged. The Smagorinsky constant c_s is set to 0.1 for the coarse mesh and 0.3 for the fine mesh, giving approximately the same peak eddy viscosity values in the island's wake ($\nu_h = 0.5$ m^{2}s^{-1}) for both meshes, in agreement with estimates by Wolanski et al. (1984). The time step is 15 seconds. All results are presented after three days of physical time in order to reach a regime situation.

4 Simple turbulence closure

In this section, the simple algebraic turbulence closure suggested by Fisher et al. (1979) and used by Deleersnijder et al. (1992) and White and Deleersnijder (2006) is presented. Accordingly, the vertical eddy viscosity ν_v is

$$\nu_v = \kappa u_* \left(h + z + z_0\right) \left(1 - \delta \frac{h + z + z_0}{H}\right), \tag{7}$$

where $\kappa \simeq 0.4$ is the von Karman constant, δ is an adjustable parameter, z_0 is the bottom roughness height and u_* is the bottom friction velocity computed as

$$u_*^2 = \frac{|\boldsymbol{\tau}|}{\rho_0} \tag{8}$$

in which ρ_0 is the water density and $\boldsymbol{\tau}$ is the bottom stress parameterised by

$$\frac{\boldsymbol{\tau}}{\rho_0} = \left(\frac{\kappa}{\ln\left(\frac{h+z+z_0}{z_0}\right)}\right)^2 |\mathbf{u}(\mathbf{z})|\, \mathbf{u}(\mathbf{z}), \tag{9}$$

where z is taken at mid-height of the first layer near the bottom. First, the δ parameter is taken to be the usual value of 0.6. This value was used in several works, including studies focusing on Rattray Island (Deleersnijder et al., 1992; White and Deleersnijder, 2006). However, using this value implies a nonzero vertical eddy viscosity at the sea surface. With the MY25 closure, the boundary condition is $\nu_v = 0$ at the sea surface when the wind stress is neglected. Obtaining a qualitatively comparable eddy viscosity profile with the simple turbulence closure requires the choice of $\delta = 1$. Results for both values of δ are presented.

Results considered in this section are taken at four different simulation times. Snapshots at these times (labelled 1 to 4) correspond respectively to December 1, 1982 at 1h40 (falling tide, peak ebb velocity), 5h00 (end of falling tide, shortly before tide reversal), 7h55 (rising tide, peak flood velocity) and 10h50

(end of rising tide, shortly before tide reversal). Figure 4 shows the depth-averaged velocity at these different times, using the model with the simple turbulence closure and $\delta = 0.6$. Trial calculations showed that the choice of turbulence closure (simple or MY25) did not significantly influence the depth-averaged horizontal velocity field. Therefore, Figure 4 gives an overview of the flow around the island that is applicable to all subsequent discussions. Figure 4 clearly shows two counter-rotating eddies of different sizes in the wake of the island. The difference between these eddies is mostly due to bathymetric effects. A study by Falconer et al. (1986) shows that when the model is run on a flat bottom, both eddies are almost symmetric in size and intensity. Our model reproduces these predictions (not shown).

Results for the upwelling velocity using the simple turbulence closure and $\delta = 0.6$ are depicted in Figure 5. Simulations on the coarse mesh give results that are slightly noisier, but not qualitatively different. Therefore, further simulations with the simple turbulence closure will only be carried out on the fine mesh. Since the model is the same as that used by White and Deleersnijder (2006), we have similar results. Using a value of $\delta = 1$ (Figure 6) has the effect of increasing the area on which upwelling is significant. The explanation is as follows. As we can see in equation (7), a larger value of δ leads to a lower value of ν_v, implying less vertical mixing. This decrease in vertical mixing gives rise to a larger vertical shear in the horizontal velocity near the bottom, inducing more intense upwelling.

5 A sophisticated turbulence closure

We have implemented the Mellor and Yamada level 2.5 (MY25) turbulence closure that was developed by Mellor and Yamada (1974, 1982). This turbulence closure includes an equation for the evolution of the variable q^2 (where $q^2/2$ is the turbulent kinetic energy), and an equation for the evolution of the variable $q^2 l$ (where l is the turbulent length scale). To have a more robust model for marine modelling, the quasi-equilibrium version of the MY25 turbulence closure was used (Galperin et al., 1988; Deleersnijder and Luyten, 1994). Since we consider a fluid of constant density, stratification is not considered in the model. The following boundary condition on q^2 is enforced both at the sea surface and at the bottom (Stacey and Pond, 1997):

$$q^2 = B_1^{2/3} u_*^2. \tag{10}$$

Note that we neglect the surface stress, which implies that we have $q^2 = 0$ at the surface. The boundary condition on the turbulent length scale, used at the bottom, is

$$l = \kappa z_0. \tag{11}$$

As in Deleersnijder et al. (1992) and White and Deleersnijder (2006), the value of the bottom roughness height z_0 is fixed to $5 \cdot 10^{-3} m$, that is typical of rough sea beds (Black and Gray, 1987). Simulations showed that variations of the bottom roughness height do not change significantly the results. At the sea surface, the boundary condition on the turbulent length scale is:

$$l = 0. \tag{12}$$

In this section, horizontal diffusion and advection of turbulence variables are not considered since they are generally deemed negligible in marine modelling compared to the more important production and destruction terms. We will investigate below how including advection affects the turbulence closure behaviour. Simulation results with the MY25 turbulence closure are shown in Figure 7. Similarly to the simple closure, simulation results are less noisy with the finest mesh. However, results using the two meshes are not qualitatively different. Now, these results will be compared with the model using the simple closure and $\delta = 1$ (Figure 6). This comparison emphasises an increase in the upwelling velocity with the MY25 model, especially for snapshots (1) and (3).

Though upwelling mechanisms are influenced by a lot of complex processes, general tendencies can nonetheless be brought to light. In order to analyse the effect of the turbulence closure scheme upon the upwelling velocity, let us consider a particular location in the two-dimensional plane where these mechanisms will be studied. This location, noted P in Figure 8, lies on the perimeter of the main eddies in the wake of the island at falling tide. Figure 9 shows the temporal evolution of the vertical eddy viscosity coefficient at P and at a depth equivalent to 90% of the total depth. Two differences between both turbulence closures are clearly visible. First, the mean eddy viscosity coefficient is slightly greater with the simple closure model. Second, there is a time lag between the two models. With the simple closure, the eddy coefficients react instantaneously when the flow changes. However, in nonstationary flows, the turbulence variables are affected by a hysteresis phenomenon. The latter has a great influence on the modeled flow during the acceleration and deceleration phases of the tide (Baumert and Radach, 1992). This hysteresis phenomenon is taken into account by the MY25 closure but not by the simple closure. In Figure 9, the time line is decomposed into two types of intervals (A and B), corresponding respectively to intervals where the vertical eddy viscosity coefficient with the MY25 model is smaller or larger than that computed by the simple closure. Figure 10 shows the bottom velocity in the y direction at P using both closures. The velocity in the y direction was chosen in lieu of the norm of the velocity in order to clearly distinguish between rising and falling tides. Moreover, the velocity in the y direction corresponds to the main component of the three-dimensional velocity during the simulation. The interesting time intervals for the study of upwelling in Figure 10 and 9 are situated in the proximity of times (1) and (2). At times (3) and (4), location P

is situated upstream of the island where there is neither eddies nor upwelling.

The effects of the MY25 closure in the A intervals are explained in Figure 11. In these zones, we have less mixing with the MY25 model yielding a larger vertical shear in the horizontal velocity. Then, the accelerations near the bottom are smaller with the MY25 closure, whereas the decelerations are larger; i.e. the bottom velocity tends to be lower with the MY25 closure. This is visible in Figure 10, mainly in (A-2) and (A-4) intervals.

Over the B intervals (Figure 11), the opposite behaviour is expected (i.e. the bottom velocity tends to be greater with the MY25 closure). In Figure 10, it is difficult to observe such a tendency. There are three possible reasons for this. First, the bottom velocity is so small in these regions, that the bottom friction has a very limited effect. Second, there is a time lag between the variations of the vertical eddy viscosity and their effect on the velocity. Third, the difference in the vertical eddy viscosity between both closures remain quite limited in these intervals (except in (B-3) where we can better observe the expected tendency).

The influence of the turbulence closure on the bottom velocity causes differences in the upwelling velocity. As the A intervals are dominant in this case, the bottom velocity is generally lower with the MY25 model. This leads to a greater vertical gradient of velocity and a more intense upwelling with the MY25 model, which can be seen by comparing Figure 6 and Figure 7.

Vertical profiles of the vertical eddy viscosity are shown in Figure 12 at the four different times. The profiles are very similar for the two models. They have the same parabolic shape, but the maximum value of the eddy viscosity on the water column is different. The difference between both closures is mainly related to the time lag and the generally larger values of the eddy viscosity coefficient for the simple closure model. These two factors influence the difference between the profiles.

To isolate the hysteresis effect, one can fix the eddy viscosity coefficient, averaged over the whole spatial and temporal domains, at the same value for the two methods. Doing so, only the hysteresis phenomena will have an effect in the comparison between both closures. This correction was made by multiplying the eddy viscosity coefficient field obtained with the MY25 model by a constant value in order to make its mean value equal to the mean eddy viscosity obtained with the simple closure model with $\delta = 1$.

Results obtained with the MY25 modified closure are shown in Figure 13. We see that, for snapshots 1, 2 and 3, the upwelling velocity increases with the MY25 modified closure in comparison with the simple closure model. However, at snapshot (4) at the end of rising tide, values of upwelling velocity are smaller with the MY25 modified model. This can be explained in Figure 14

showing the temporal evolution of the vertical eddy viscosity coefficient at P and at a depth of 90% near the bottom. We can see that the only effect is the time lag. The MY25 modified closure responds with a delay compared with the simple closure. The consequence is that, at the beginning of the tides (A intervals), the MY25 modified closure gives less mixing than the simple closure model. The upwelling at these times tends to be more important for the MY25 modified closure. However, before tide reversal (B intervals), the MY25 modified closure gives more mixing than the simple closure model. This is particularly visible at snapshot (4). At this moment, the upwelling velocity is less important compared with the simple closure model.

The time lag effect can cause differences in the upwelling velocity, but since these differences can be positive or negative, they do not necessarily lead to a global increase or decrease in upwelling. This time lag may be substantial and can reach up to one hour.

6 Discussion

To see if the predicted upwelling would be sufficient to carry the sediments from the sea bed to the sea surface within an eddy, the upwelling velocity can be time-integrated during the course of a tidal cycle. This integration yields what we will define as an upwelling height, and takes into account both upwelling and downwelling that can occur during the integration period. This integration was carried out at a location (noted Q in Figure 15), situated in a high upwelling zone at falling tide. The results of the time integration of the upwelling velocities are shown on Table 1. As the depth at Q is about 25 m, we can reasonably assume that only the MY25 and the MY25 modified closures will be able to account for the vertical transport throughout the water column during the period considered. However, this diagnosis is based on restrictive hypotheses. First, we use the upwelling velocity at mid-depth where it typically reaches its maximum value. Second, the integration of the upwelling velocity does not take into account the horizontal transport. By resorting to the theory of the age (Delhez et al., 1999; Deleersnijder et al., 2001), the study by White and Deleersnijder (2006) showed that horizontal transport could be crucial in explaining upwelling mechanisms. Nevertheless, the time integration of the upwelling velocity can give a good idea of the capacity of the vertical flow to carry the sediments to the sea surface within eddies.

It is often assumed that the characteristic time is much larger for the advection of turbulence variables than for the production/destruction terms. If so, the advection term can be regarded as negligible. At smaller scales, this term could be more important, particularly for complex bathymetries. There we study the influence of the advection term of turbulence variables upon the

upwelling velocity. Figure 16 shows the upwelling velocity at four different times, obtained from the simulation using the MY25 closure with advection of turbulence variables. The simulations are performed with the coarse mesh. In comparison with Figure 7, we can see that advection of turbulence variables has a small influence on the results. This can be understood with an order of magnitude analysis of the different terms influencing the evolution of the turbulent kinetic energy. The simulation results show that the advection has an influence that is on average 10 times less important than the production/destruction terms. Vertical diffusion is almost of the same order of magnitude as the production/destruction term. In the context of Rattray Island and similar problems, the advection of turbulence variables has a limited effect and can be neglected. It might, however, be important in other configurations, especially for flow characterised by smaller horizontal scales.

7 Conclusion

In this work, a Mellor and Yamada level 2.5 (MY25) turbulence closure was implemented in a three-dimensional finite element hydrodynamic marine model. Simulations were performed around Rattray Island, in order to estimate the effect of the turbulence closure on the upwelling velocity in the wake of the island.

The upwelling velocity is significantly altered when using the MY25 closure instead of a simple algebraic closure. This difference is mostly caused by two factors. First, the vertical eddy viscosity is, on average, smaller with MY25. This leads to less mixing and a larger vertical shear in the horizontal velocity at the bottom. As a consequence, this tends to increase upwelling in the centre of the eddies. The second reason is that the MY25 closure takes into account the hysteresis effect on turbulence variables. This hysteresis effect induces a delay in the variation of turbulence variables, which has an influence on the upwelling velocity. This influence can, depending on the situation, increase or decrease the upwelling. The shape of the vertical profiles of eddy viscosity are quite similar with both closures.

The MY25 closure gives sufficient upwelling in the wake of the island to reasonably explain the transport of sediments from the sea bottom to the sea surface. This is not the case with the model using the simple turbulence closure. However, a diagnosis based on the age (White and Deleersnijder, 2006) accounted for the presence of mud at the surface via intense upwelling off the tips of the island. The high turbidity downstream of the island is possibly due to the combination of upwelling in the centre of the eddies and vertical transport near the tips of the island.

A simulation was performed with advection of turbulence variables in order to estimate its effect on smaller scale. In the case of the tidal circulation around a shallow-water island, the effect of advection of turbulence variables is relatively small and can be neglected. This conclusion was confirmed by an analysis of orders of magnitude carried out on the turbulent kinetic energy equation.

The Mellor and Yamada level 2.5 turbulence closure improves the model in its ability to predict upwelling. The sophistication level of MY25 is not mandatory for a non-stratified problem such as Rattray Island, yet it brings to light phenomena that are simply absent when using a simple algebraic closure.

8 Acknowledgements

Sébastien Blaise is a Research fellow with the Belgian Fund for Research in Industry and Agriculture (FRIA). Laurent White and Eric Deleersnijder are a Research fellow and a Research associate, respectively, with the Belgian National Fund for Scientific Research (FNRS). The present study was carried out within the scope of the project "A second-generation model of the ocean system", which is funded by the *Communauté Francaise de Belgique*, as *Actions de Recherche Concertées*, under contract ARC 04/09-316. This work is a contribution to the development of SLIM, the Second-generation Louvain-la-Neuve Ice-ocean Model (http://www.climate.be/SLIM). The authors indebted to Eric Wolanski for providing data concerning Rattray Island.

References

Aikman, F., Baptista, A., Blain, C., Iskandarani, M., 2006. Cross-scale Ocean Modelling Benchmark. WWW Page, *http://www.stccmop.org/node/114*.

Akin, J., Tezduyar, T., Ungor, M., Mittal, S., 2003. Stabilization parameters and Smagorinsky turbulence model. *Journal of Applied Mechanics* 70 (1), 1–9.

Baumert, H., Radach, G., 1992. Hysteresis of Turbulent Kinetic Energy in Nonrotational Tidal Flows: A Model Study. *Journal of Geophysical Research* 97, 3669–3677.

Black, K., Gray, S., 1987. Eddy formation in unsteady flows. *Journal of Geophysical Research* 92 (C9), 9514–9522.

Blaise, S., White, L., 2006. Development of a marine modelling benchmark: tidal circulation around Rattray Island. WWW Page, *http://www.climate.be/SLIM/Benchmarks*.

Blumberg, A., Galperin, B., 2006. Modeling Vertical Structure of Open-Channel Flows. *Journal of Hydraulic Engineering* 118 (8), 1119–1134.

Bowker, K. A., 1988. Albert Einstein and meandering rivers. *Earth Science History* 7 (1), 45–46.

Burchard, H., 2002. *Applied Turbulence Modelling in Marine Waters,* vol. 100 of *Lecture Notes in Earth Sciences*. *Springer, Berlin, Heidelberg, New York*.

Cushman-Roisin, B., Naimie, C. E., 2002. A 3D finite-element model of the Adriatic tides. *Journal of Marine Systems* 37 (4), 279–297.

Danilov, S., Kivman, G., Schröter, J., 2004. A finite element ocean model: principles and evaluation. *Ocean Modelling* 6, 125–150.

Danilov, S., Kivman, G., Schröter, J., 2005. Evaluation of an eddy-permitting finite-element ocean model in the North Atlantic. *Ocean Modelling* 10, 35–49.

Deleersnijder, E., 1989. Upwelling and upsloping in three-dimensional marine models. *Applied Mathematical Modelling* 13, 462–467.

Deleersnijder, E., 1994. An analysis of the vertical velocity field computed by a three-dimensional model in the region of the Bering Strait. *Tellus A* 46, 149–159.

Deleersnijder, E., Campin, J.-M., Delhez, E. J. M., 2001. The concept of age in marine modelling: I. Theory and preliminary results. *Journal of Marine Systems* 28, 229–267.

Deleersnijder, E., Luyten, P., 1994. On the practical advantages of the quasi-equilibrium version of the Mellor and Yamada level 2.5 turbulence closure applied to marine modelling. *Applied Mathematical Modelling* 18, 281–287.

Deleersnijder, E., Norro, A., Wolanski, E., 1992. A three-dimensional model of the water circulation around an island in shallow water. *Continental Shelf Research* 12 (7/8), 891–906.

Delhez, E. J. M., Campin, J.-M., Hirst, A. C., Deleersnijder, E., 1999. Toward a general theory of the age in ocean modelling. *Ocean Modelling* 1, 17–27.

Ezer, T., 2005. Entrainment, diapycnal mixing and transport in three-

dimensional bottom gravity current simulations using the Mellor-Yamada turbulence scheme. *Ocean Modelling* 9, 151–168.

Falconer, R., Wolanski, E., Mardapitta-Hadjipandeli, L., 1986. Modeling tidal circulation in an island's wake. *Journal of Waterway, Port, Coastal and Ocean Engineering* 112, 234–254.

Fisher, H., List, J., Koh, C., Imberger, J., Brooks, N., 1979. *Mixing in Inland and Coastal Waters. Academic Press, New York.*

Flather, R., 1976. A tidal model of the northwest European continental shelf. *Mémoires de la Société Royale des Sciences de Liège* 6(10), 141–164.

Ford, R., Pain, C. C., Piggott, M. D., Goddard, A. J. H., de Oliveira, C. R. E., Umpleby, A. P., 2004a. A non-hydrostatic finite element model for three-dimensional stratified oceanic flows. Part I: model formulation. *Monthly Weather Review* 132, 2816–2831.

Ford, R., Pain, C. C., Piggott, M. D., Goddard, A. J. H., de Oliveira, C. R. E., Umpleby, A. P., 2004b. A non-hydrostatic finite element model for three-dimensional stratified oceanic flows. Part II: model validation. *Monthly Weather Review* 132, 2832–2844.

Fortunato, A. B., Baptista, A. M., Luettich, R. A., 1997. A three-dimensional model of tidal currents in the mouth of the Tagus estuary. *Continental Shelf Research* 17 (14), 1689–1714.

Galperin, B., Kantha, L., Hassid, S., Rosati, A., 1988. A quasi-equilibrium turbulent energy model for geophysical flows. *Journal of the Atmospheric Sciences* 45, 55–62.

Gorman, G. J., Piggott, M. D., Pain, C. C., de Oliveira, C. R. E., Umpleby, A. P., Goddard, A. J. H., 2006. Optimisation based bathymetry approximation through constrained unstructured mesh adaptivity. *Ocean Modelling* 12, 436–452.

Hanert, E., Deleersnijder, E., Legat, V., 2006. An adaptative finite element water column model using the Mellor-Yamada level 2.5 turbulent closure scheme. *Ocean Modelling* 12, 205–223.

Hanert, E., Legat, V., Deleersnijder, E., 2003. A comparison of three finite elements to solve the linear shallow water equations. *Ocean Modelling* 5, 17–35.

Hanert, E., Roux, D. Y. L., Legat, V., Deleersnijder, E., 2005. An efficient Eulerian finite element method for the shallow water equations. *Ocean Modelling* 10, 115–136.

Kinnmark, I., 1986. The Shallow Water Wave Equations: Formulation, Analysis and Applications. Vol. 15 of Lecture Notes in Engineering. Springer-Verlag.

Kolar, R. L., Westerink, J. J., Cantekin, M. E., Blain, C. A., 1994. Aspects of nonlinear simulations using shallow-water models based on the wave continuity equation. *Computers and Fluids* 23 (3), 523–538.

Labeur, R., Pietrzak, J., 2005. A fully three dimensional unstructured grid non-hydrostatic finite element coastal model. *Ocean Modelling* 10, 51–67.

Le Roux, D. Y., 2001. A new triangular finite-element with optimum constraint

ratio for compressible fluids. *SIAM Journal on Scientific Computing* 23 (1), 66–80.

Le Roux, D. Y., 2005. Dispersion relation analysis of the $P_1^{NC} - P_1$ finite-element pair in shallow-water models. *SIAM Journal on Scientific Computing* 27 (2), 394–414.

Le Roux, D. Y., Staniforth, A., Lin, C. A., 1998. Finite elements for shallow-water equation ocean models. *Monthly Weather Review* 126, 1931–1951.

Legrand, S., Deleersnijder, E., Delhez, E., Legat, V., 2007. Unstructured, anisotropic mesh generation for the Northwestern European continental shelf, the continental slope and the neighboring ocean. *Continental Shelf Research* 27, 1344–1356.

Legrand, S., Deleersnijder, E., Hanert, E., Legat, V., Wolanski, E., 2006. High-resolution unstructured meshes for hydrodynamic models of the Great Barrier Reef, Australia. *Estuarine, Coastal and Shelf Science* 68, 36–46.

Legrand, S., Legat, V., Deleersnijder, E., 2000. Delaunay mesh generation for unstructured-grid ocean general circulation model. *Ocean Modelling* 2, 17–28.

Lynch, D., Ip, J., Naimie, C., Werner, F., 1996. Comprehensive coastal circulation model with application to the Gulf of Maine. *Continental Shelf Research* 16, 875–906.

Lynch, D. R., Gray, W. R., 1979. A wave equation model for finite element tidal computations. *Computers and Fluids* 7, 207–228.

Lynch, D. R., Naimie, C. E., 1993. The M2 tide and its residuals on the outer banks of the Gulf of Maine. *Journal of Physical Oceanography* 23, 2222–2253.

Massey, T. C., Blain, C. A., 2006. In search of a consistent and conservative mass flux for the GWCE. *Computer Methods in Applied Mechanics and Engineering* 195, 571–587.

Mellor, G. L., Yamada, T., 1974. A hierarchy of turbulence closure models for planetary boundary layers. *Journal of the Atmospheric Sciences* 31, 1791–1806.

Mellor, G. L., Yamada, T., 1982. Development of a turbulence closure model for geophysical fluid problems. *Review of Geophysics and Space Physics* 20, 851–875.

Nechaev, D., Schröter, J., Yaremchuk, M., 2003. A diagnostic stabilized finite-element ocean circulation model. *Ocean Modelling* 5, 37–63.

Pain, C. C., Piggott, M., Goddard, A., Fang, F., Gorman, G., Marshall, D. P., Eaton, M., Power, P., de Oliveira, C., 2005. Three-dimensional unstructured mesh ocean modelling. *Ocean Modelling* 10, 5–33.

Pietrzak, J., Deleersnijder, E., Schröter, J., 2005. Special Issue: The Second International Workshop on Unstructured Mesh Numerical Modelling of Coastal, Shelf and Ocean Flows. *Ocean Modelling* 10, 1–252.

Pietrzak, J., Iskandarani, M., Schröter, J., Lyard, F., 2006. Special Issue: The Third International Workshop on Unstructured Mesh Numerical Modelling of Coastal, Shelf and Ocean Flows. *Ocean Modelling* 15, 1–138.

Ruddick, K., Deleersnijder, E., Luyten, P., Ozer, J., 1995. Haline stratification in the Rhine-Meuse freshwater model sensitivity analysis. *Continental Shelf Research* 15, 1597–1630.

Ruddick, K., Deleersnijder, E., Mulder, T. D., Luyten, P., 1994. HA model study of the Rhine discharge front and downwelling circulation. *Tellus Ser. A* 46, 149–159.

Smagorinsky, J., 1963. General circulation experiments with the primitive equations. 1 The basic experiments. *Monthy Weather Review* 91 (5), 99–165.

Stacey, M. W., Pond, S., 1997. On the Mellor-Yamada Turbulence Closure Scheme: The Surface Boundary Condition for q^2. *Journal of Physical Oceanography* 27, 2081–2086.

Timmermann, R., Losch, M., 2005. Using the Mellor-Yamada mixing scheme in seasonally ice-covered seas-Corrigendum to: Parameterization of vertical mixing in the Weddell Sea. *Ocean Modelling* 10, 369–372.

Walters, R. A., 2006. Design considerations for a finite element coastal ocean model. *Ocean Modelling* 15, 90–100.

Walters, R. A., Werner, F. E., 1989. A comparison of two finite element models of tidal hydrodynamics using the North Sea data set. *Advances in Water Resources* 12, 184–193.

White, L., Deleersnijder, E., 2006. Diagnoses of vertical transport in a three-dimensional finite-element model of the tidal circulation around an island. *Estuarine, Coastal and Shelf Science* (in press).

White, L., Deleersnijder, E., Legat, V., 2007. A Three-Dimensional Unstructured Mesh Finite Element Marine Model, With Application to the Flow Around a Shallow-Water Island. *Ocean Modelling, in preparation.*

Wolanski, E., Asaeda, T., Tanaka, A., Deleersnijder, E., 1996. Three-dimensional island wakes in the field, laboratory experiments and numerical models. *Continental Shelf Research* 16 (11), 1437–1452.

Wolanski, E., Hamner, W., 1988. Topographically controlled fronts in ocean and their biological influence. *Science* 241 (4862), 177–181.

Wolanski, E., Imberger, J., Heron, M., 1984. Island wakes in Shallow Waters. *Journal of Geophysical Research* 89 (C6), 10553–10569.

List of Figures

Turbulence model	Upwelling height $[m]$
Simple closure, $\delta = 0.6$	11.5
Simple closure, $\delta = 1$	19.6
MY25 modified	24.6
MY25	30.1

Table 1
Time-integration over a tide period of the upwelling velocity at mid-depth on Q position. Integration started on December 1, 1982 at 0h55 and ended at 7h05, the same day.

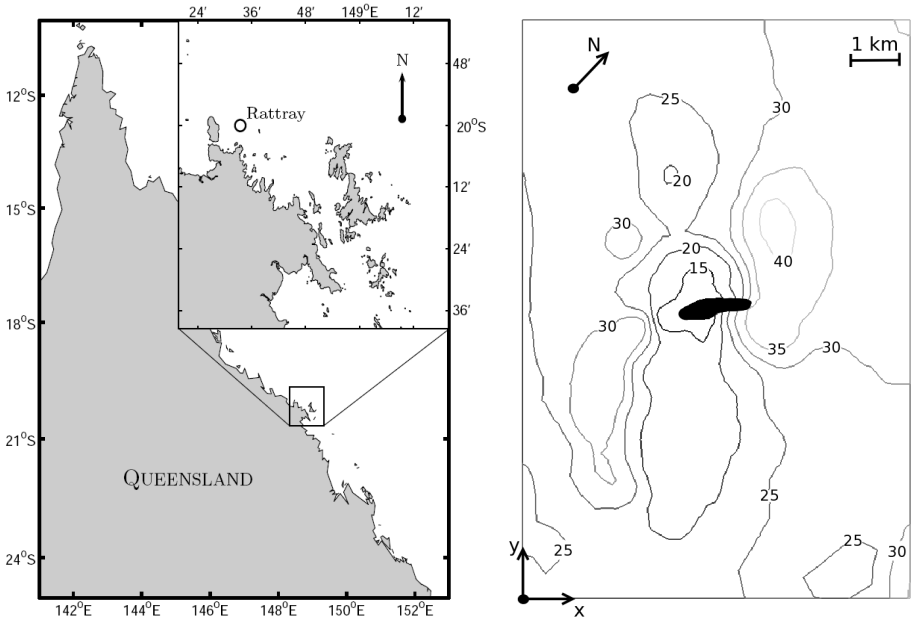

Fig. 1. Left: location of Rattray Island in the Great Barrier Reef, Northeast Australia. Right: domain of interest with bathymetry in metres. Rattray Island is the black area in the centre. (from White et al., 2007)

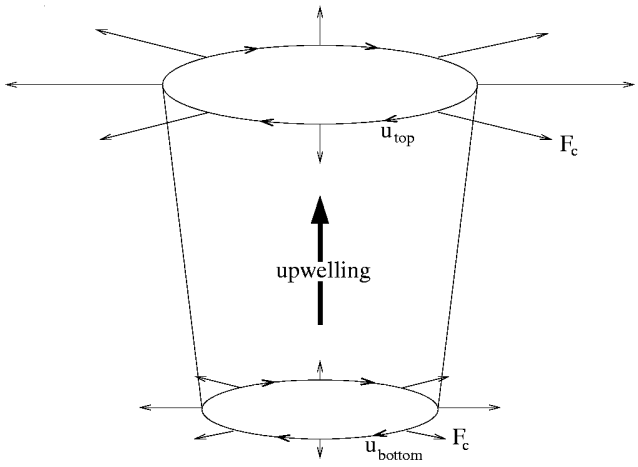

Fig. 2. Schematic illustration of the mechanism of the upwelling induced in the centre of an eddy. F_c is the centrifugal acceleration due to the rotating velocity on the top (u_{top}) and on the bottom (u_{bottom}) perimeters of the eddy.

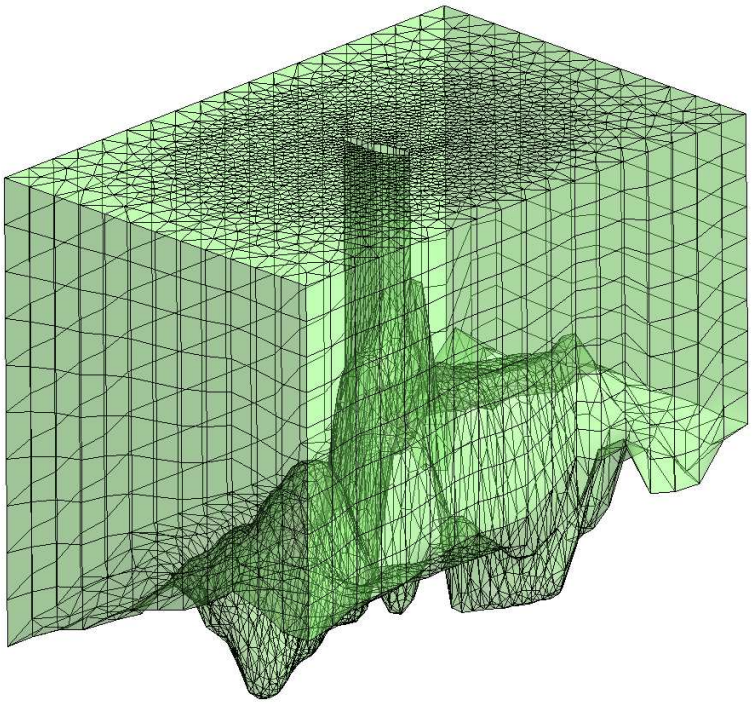

Fig. 3. Coarsest unstructured mesh used for the simulations. The mesh contains 3024 triangles and 10 layers on the vertical. To better render the bathymetry, a stretch is applied in the vertical direction.

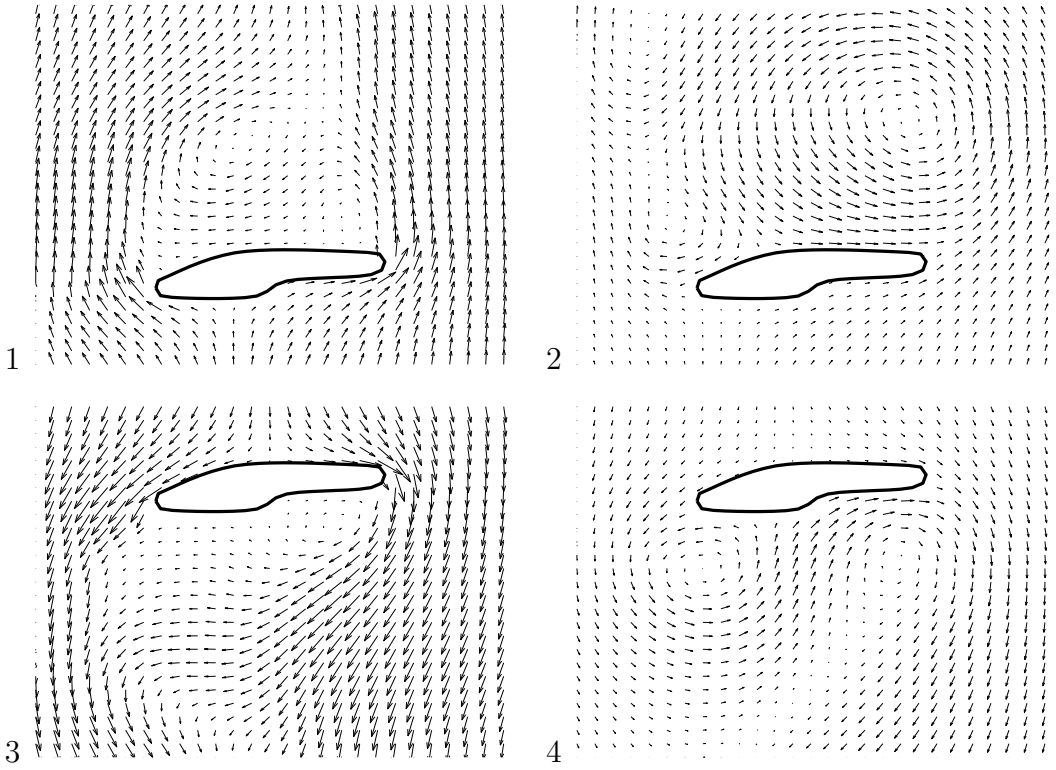

Fig. 4. Depth-averaged velocity field on the fine mesh, using the model with simple turbulence closure with the parameter $\delta = 0.6$. Snapshots (1,2,3 and 4) respectively taken on December 1, 1982 at 1h40 (falling tide, peak ebb velocity), 5h00 (end of falling tide, shortly before tide reversal), 7h55 (rising tide, peak flood velocity) and 10h50 (end of rising tide, shortly before tide reversal). The velocity has been interpolated on a structured mesh. The mean velocity in the y-direction at snapshots (1,2,3 and 4) is respectively $0.49m/s$, $0.16m/s$, $-0.52m/s$ and $-0.16m/s$.

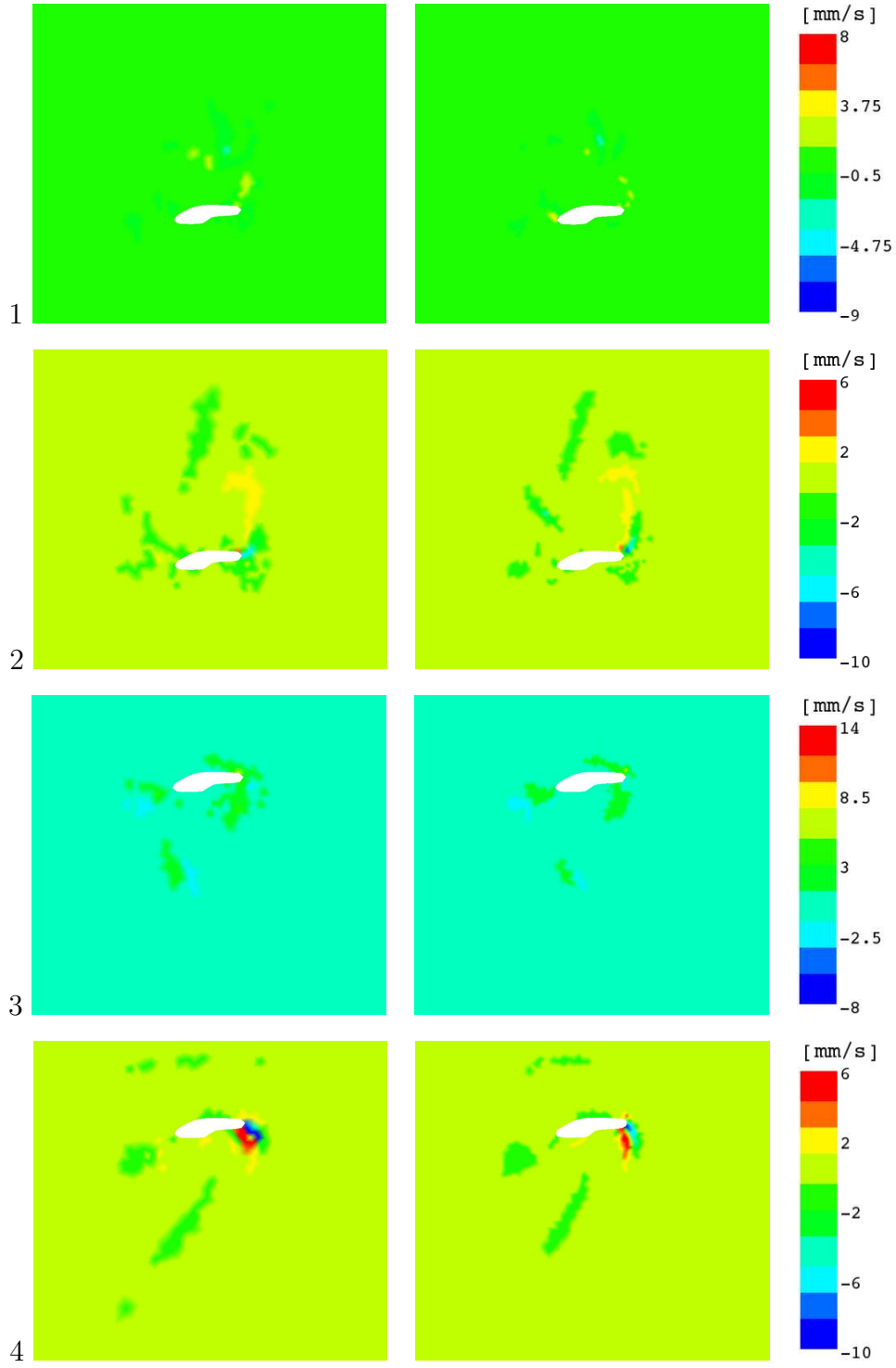

Fig. 5. Upwelling velocity at mid-depth for the coarse mesh (left column) and for the fine mesh (right column), using the simple turbulence closure with the parameter $\delta = 0.6$. Snapshots (1,2,3 and 4) respectively taken on December 1, 1982 at 1h40 (falling tide, peak ebb velocity), 5h00 (end of falling tide, shortly before tide reversal), 7h55 (rising tide, peak flood velocity) and 10h50 (end of rising tide, shortly before tide reversal).

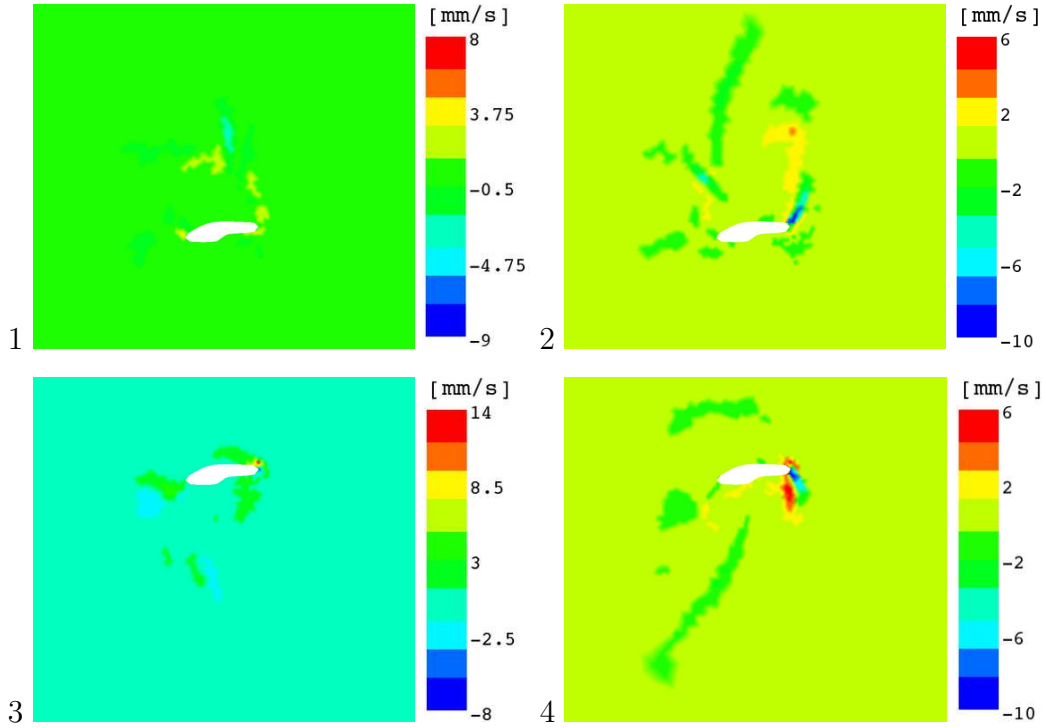

Fig. 6. Upwelling velocity at mid-depth for the fine mesh, using the simple turbulence closure with the parameter $\delta = 1$. Snapshots (1,2,3 and 4) respectively taken on December 1, 1982 at 1h40 (falling tide, peak ebb velocity), 5h00 (end of falling tide, shortly before tide reversal), 7h55 (rising tide, peak flood velocity) and 10h50 (end of rising tide, shortly before tide reversal).

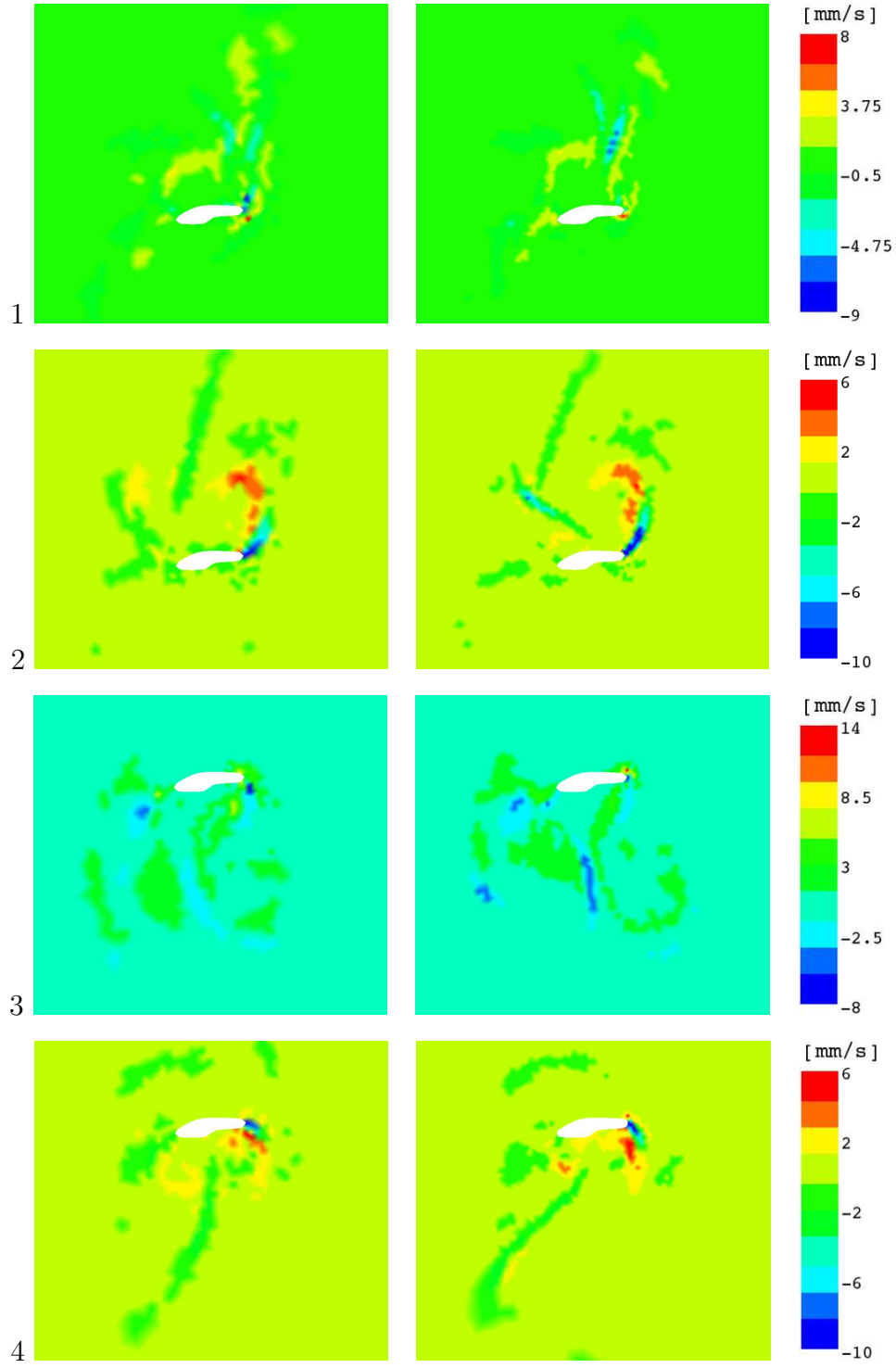

Fig. 7. Upwelling velocity at mid-depth for the coarse mesh (left column) and for the fine mesh (right column), using the Mellor and Yamada level 2.5 turbulence closure. Snapshots (1,2,3 and 4) respectively taken on December 1, 1982 at 1h40 (falling tide, peak ebb velocity), 5h00 (end of falling tide, shortly before tide reversal), 7h55 (rising tide, peak flood velocity) and 10h50 (end of rising tide, shortly before tide reversal).

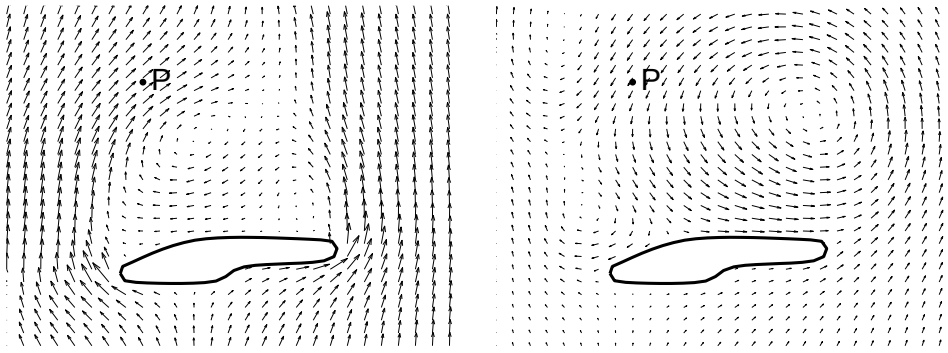

Fig. 8. Position of the water column where temporal plots of velocity and eddy viscosity are studied. P is located on the perimeter of the eddy at falling tide. Snapshots (1,2) taken respectively on December 1, 1982 at 1h40 (falling tide, peak ebb velocity) and 5h00 (end of falling tide, shortly before tide reversal).

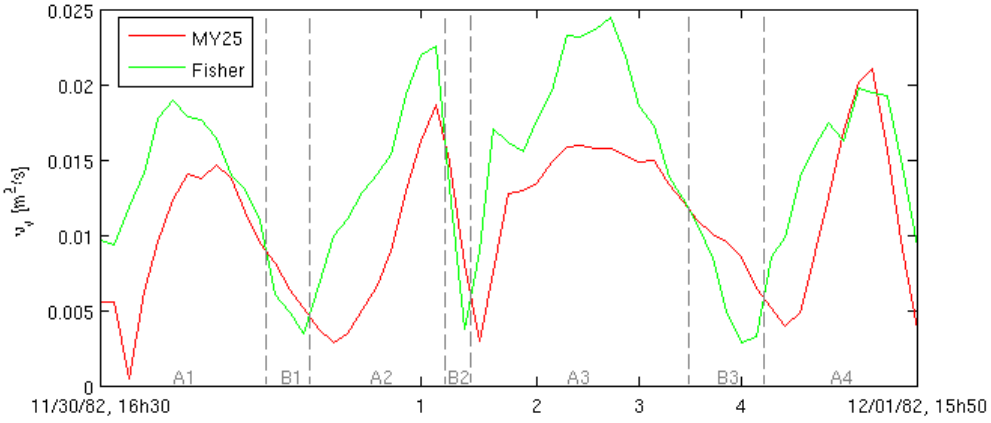

Fig. 9. Temporal evolution of the eddy viscosity at a depth of 90% near the bottom and at P position. Comparison between the Mellor and Yamada level 2.5 turbulence closure and the simple turbulence closure (Fisher) with $\delta = 1$. Times (1,2,3 and 4) correspond respectively to December 1, 1982 at 1h40 (falling tide, peak ebb velocity), 5h00 (end of falling tide, shortly before tide reversal), 7h55 (rising tide, peak flood velocity) and 10h50 (end of rising tide, shortly before tide reversal).

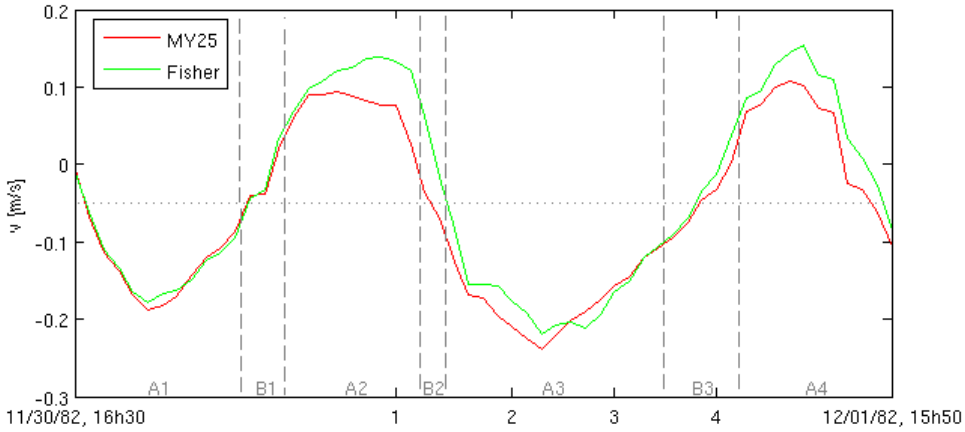

Fig. 10. Temporal evolution of the bottom velocity at P position. Comparison between the Mellor and Yamada level 2.5 turbulence closure and the simple turbulence closure (Fisher) with $\delta = 1$. Times (1,2,3 and 4) correspond respectively to December 1, 1982 at 1h40 (falling tide, peak ebb velocity), 5h00 (end of falling tide, shortly before tide reversal), 7h55 (rising tide, peak flood velocity) and 10h50 (end of rising tide, shortly before tide reversal).

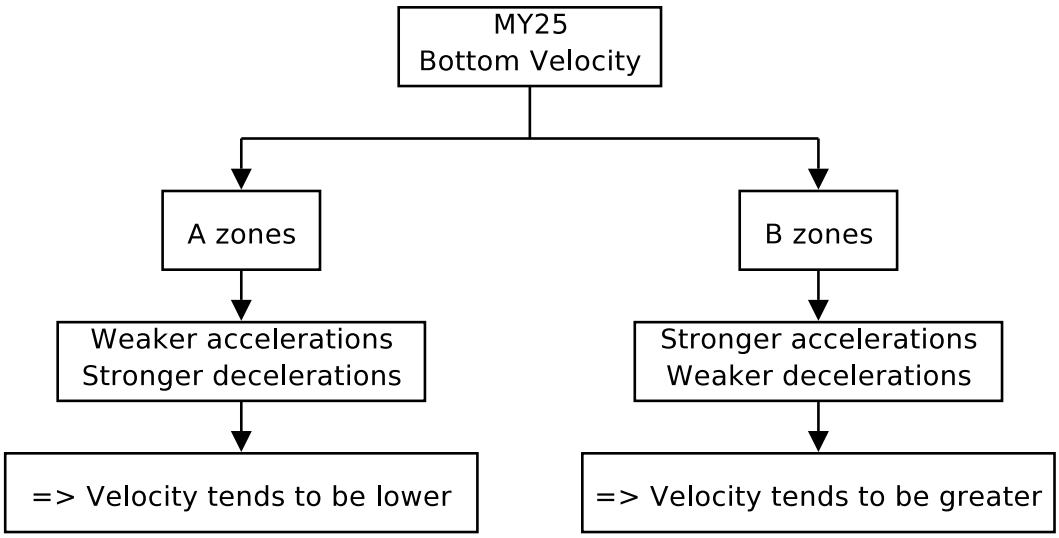

Fig. 11. Effects on the bottom velocity due to the MY25 model.

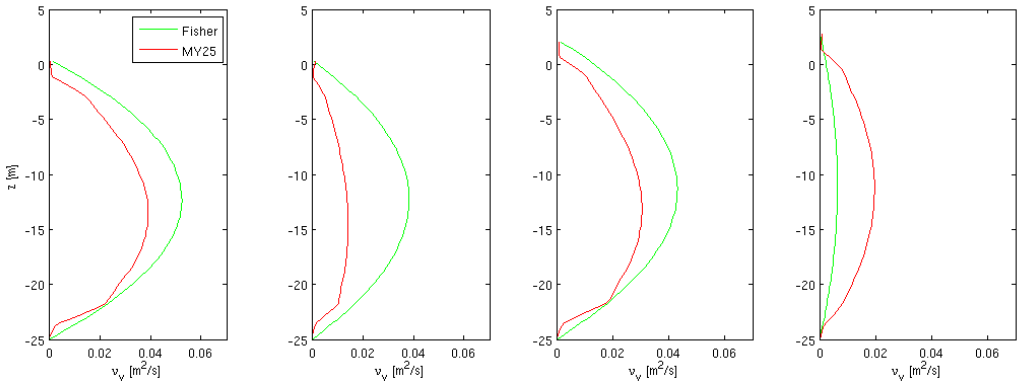

Fig. 12. Vertical profile of vertical eddy viscosity at P position. Comparison between the Mellor and Yamada level 2.5 turbulence closure and the simple turbulence closure (Fisher) with $\delta = 1$. Snapshots (1,2,3 and 4) respectively taken on December 1, 1982 at 1h40 (falling tide, peak ebb velocity), 5h00 (end of falling tide, shortly before tide reversal), 7h55 (rising tide, peak flood velocity) and 10h50 (end of rising tide, shortly before tide reversal).

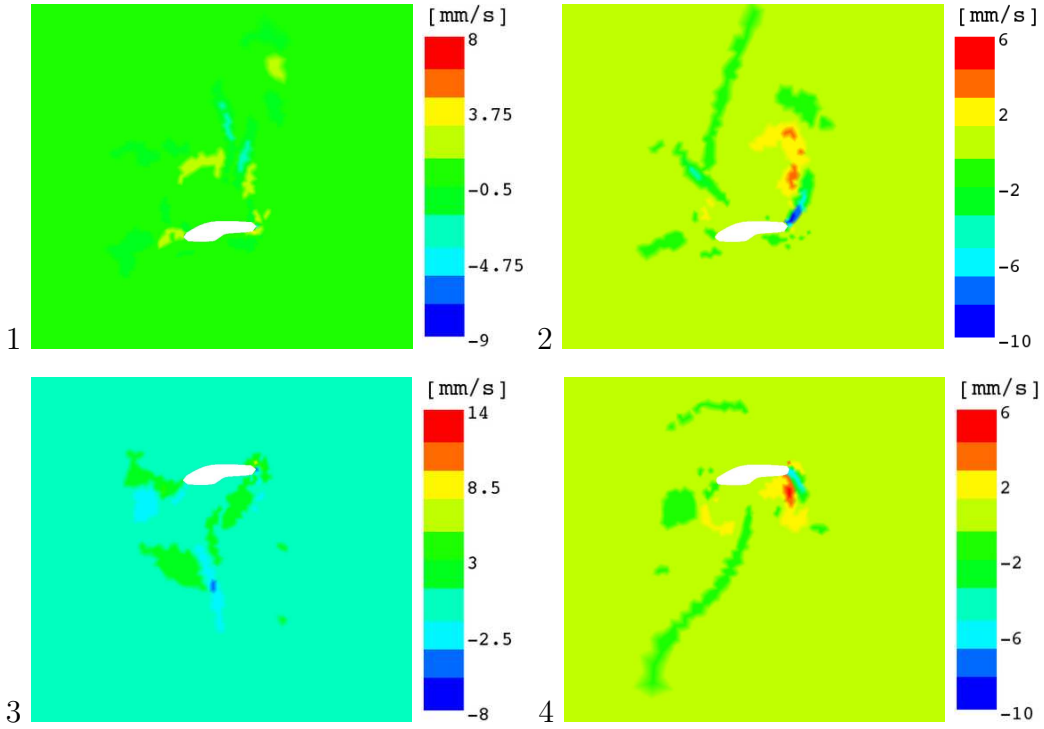

Fig. 13. Upwelling velocity at mid-depth for the fine mesh, using the Mellor and Yamada level 2.5 turbulence closure with modified vertical eddy viscosity in order to have the same mean value than using the simple turbulence closure. Snapshots (1,2,3 and 4) respectively taken on December 1, 1982 at 1h40 (falling tide, peak ebb velocity), 5h00 (end of falling tide, shortly before tide reversal), 7h55 (rising tide, peak flood velocity) and 10h50 (end of rising tide, shortly before tide reversal).

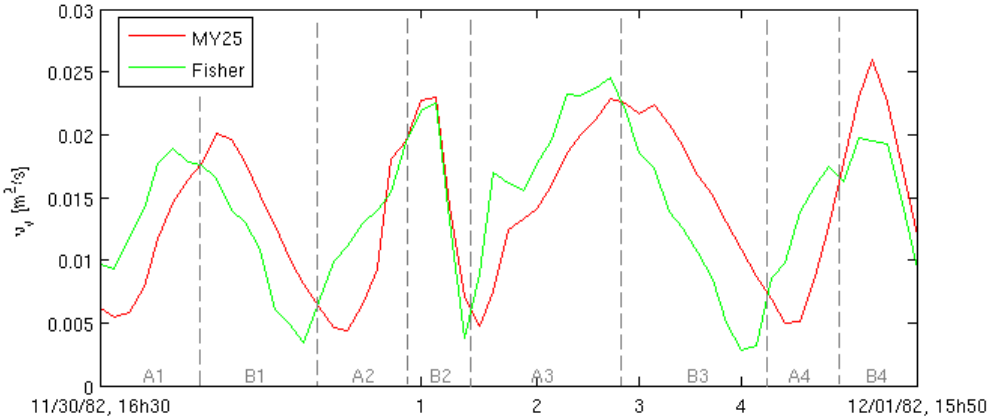

Fig. 14. Temporal evolution of the eddy viscosity at a depth of 90% near the bottom and at P position. Comparison between the Mellor and Yamada level 2.5 turbulence closure with a multiplicative factor for ν_v and the simple turbulence closure (Fisher) with $\delta = 1$. Times (1,2,3 and 4) correspond respectively to December 1, 1982 at 1h40 (falling tide, peak ebb velocity), 5h00 (end of falling tide, shortly before tide reversal), 7h55 (rising tide, peak flood velocity) and 10h50 (end of rising tide, shortly before tide reversal).

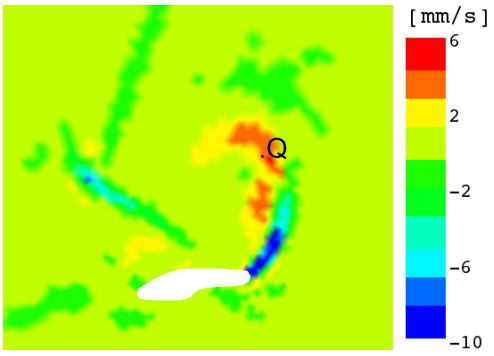

Fig. 15. Position of the water column where the upwelling velocity is time-integrated over a tide period. Snapshot taken on December 1, 1982 at 5h00 (end of falling tide, shortly before tide reversal) with the Mellor and Yamada level 2.5 turbulence closure.

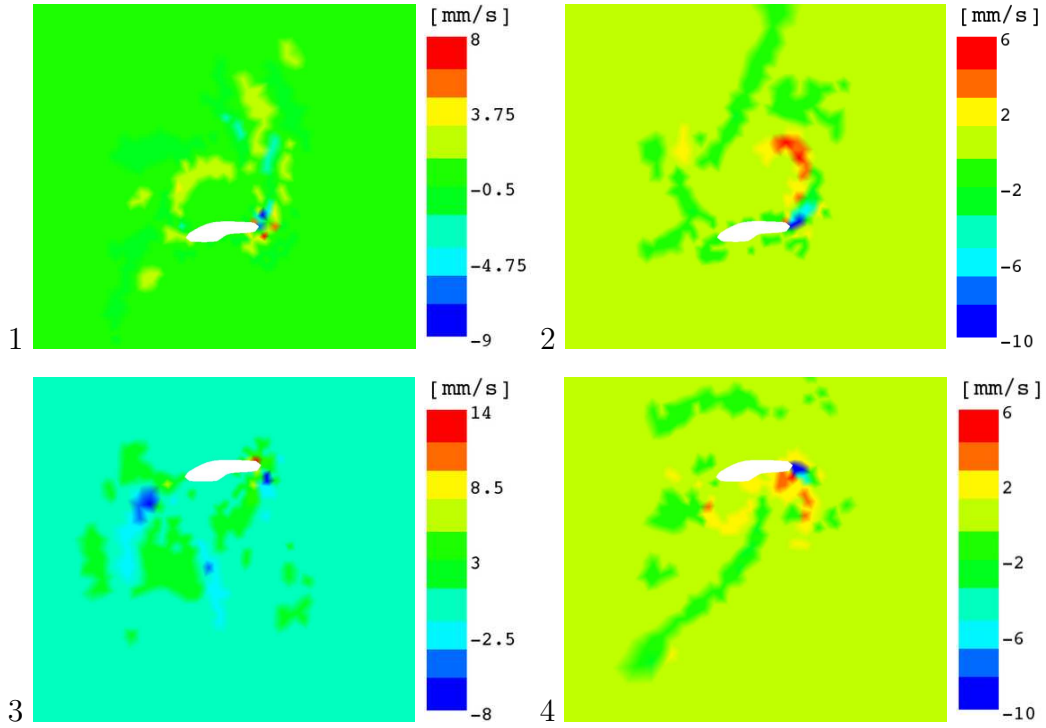

Fig. 16. Upwelling velocity at mid-depth for the coarse mesh, using the Mellor and Yamada level 2.5 turbulence closure with advection of turbulence variables. Snapshots (1,2,3 and 4) respectively taken on December 1, 1982 at 1h40 (falling tide, peak ebb velocity), 5h00 (end of falling tide, shortly before tide reversal), 7h55 (rising tide, peak flood velocity) and 10h50 (end of rising tide, shortly before tide reversal).